

Original Article | ISSN (0): 2582-631X

DOI: 10.47857/irjms.2025.v06i04.06817

Impact of High Heat Input on Micro-Structural and Mechanical Performance of SS304L/DSS2205 Steel Dissimilar GTA Weld

Gyanendu Sharma*, Bhupendra Singh Chauhan

Department of Mechanical Engineering, GLA University, Mathura, Uttar-Pradesh, India. *Corresponding Author's Email: gyanendusharma2005@gmail.com

Abstract

The impact of heat input on dissimilar welded joints plates composed of stainless (Stnls) steel (SS304L) and duplex Stnls steel (DSS 2205) is the prime segment of this study. When employing ER309L & ER 2209 filler in the gas filled tungsten arc welding (GTAW), one heat input was chosen as the higher heat input (HHI) (1.404 kJ/mm) that was desired. Heat input ranged from 150-195A with 14-16V voltage. Both the HAZ and the weld zone exhibit macro segregation, resembling islands and peninsulas. The ferrite content of the HHI weld zone falls as heat input rises. However, austenite nucleation in the HAZ was positively impacted by HHI. The 309L HAZ micro-hardness increases from 203.63 Hv 0.5 to 281.91 Hv 0.5; likewise, the 2209 filler micro-hardness increases from 246.72 Hv 0.5 to 283.94 Hv 0.5 horizontally from WZ to HAZ. For 309L and 2209 filler, the HHI weldments' tensile strength parameter, or maximum force, was 27052N and 27389.8N, respectively. Observation of WA, PTA, GBA, RA found during characterization. During impact test fracture analysis we observe parabolic dimples, teat ridges, micro voids which emboldened the high ductile nature of the joint. Ferrite-austenite phase transformation has sought secondary austenite in the post weld coupon. Tests like the tensile testing; Charpy impact testing and Vickers micro-hardness testing were performed to determine mechanical properties of the dissimilar metal welds (DMWs).

Keywords: Dissimilar Weld, Duplex Stainless Steel, Filler Metal, High Heat Input, Microstructure.

Introduction

To fully utilize two distinct metals with different mechanical, metallurgical, and physical properties, a dissimilar steel metal joint is preferred TIG welding applications in many sectors, particularly industries which enormously used under engineering and cost efficient zone such as the automotive sector, power plant sector, and petrochemical sector (1). Given the importance of dissimilar metal joints, duplex stainless steel (DSS 2205) and austenitic stainless steel (SS304L) grades of the utmost quality have become more common in present decade industrial applications for dissimilar welding by fusion welding, primarily for technical and financial reasons. Better fatigue strength, increased tensile and impact toughness, enhanced resistance to SCC (stress corrosion cracking), pitting, and widespread corrosion are just a few of DSS 2205 exceptional mechanical qualities. Its balanced ferrite and austenite dual phase which gives these steel composition fitting weld-ability and formability. The study also used stainless steel (304L), which is frequently used in

subsea and oil gas equipment. The microstructure of SS304L is made up of some annealed processed twins, carbide precipitation at previous austenite (gamma-γ) grain boundaries, and a single-phase γ grain (FCC, c) with delta (δ)-ferrite. A better material for seawater applications, SS304L also exhibits higher ductility, enhanced tensile strength and impact (sudden blow) toughness, improved corrosion characteristics, when compared to its other stainless steel (SS) grades, such as 308, 310, 316 (2). Maintaining the proper phase balance between delta and gamma is crucial when welding DSS 2205 (3). By employing solution annealing, regulated heat infusion (HI) and rate of cooling, and maintain fertilization at very high (°C) temperature, the retention of the gamma to delta phase balance during the metal joining (welding) process may be managed. Due to the presence of alloying components, the intermetallic phase production rate varies with temperature (4). By achieving the weld delta/gamma ratio, intermetallic phases in DSS 2205 weldment can be

This is an Open Access article distributed under the terms of the Creative Commons Attribution CC BY license (http://creativecommons.org/licenses/by/4.0/), which permits unrestricted reuse, distribution, and reproduction in any medium, provided the original work is properly cited.

(Received 09th July 2025; Accepted 02nd October 2025; Published 30th October 2025)

reduced or eliminated with the right heat infusion and rate of cooling management. The degradation of corrosion and mechanical qualities is one of the well-documented concerns with DSS 2205. These result from the production of coarse material grains, too much rate of cooling, thermal cycles, chemical composition, and improper HI. Finding the HI property connection between the dissimilar joints of DSS 2205 and SS304L is therefore The link between the joint's essential. microstructural and mechanical properties has, however, received very little research (5). The intended balance of dual phases in between delta and gamma is achieved by some researchers. Welding DSS 2205 requires a regulated heat input (6). Higher heat input causes the creation of brittle inter-metallic phases like chi or sigma. They have found that slower cooling rates result in intermetallic phase development and grain coarsening at HAZ, while quicker cooling rates generate low austenite reformation and Cr2N precipitation. Because of the current precipitation of Cr2N and sigma phase, meanwhile the sigma phase is a preferred nucleation site for the precipitation of inter-metallic compounds researchers have noted that inappropriate HI affects corrosion distinctiveness (12,13). Rise in HI assisted in reducing the ferrite (delta (δ)) concentration by sufficient ferrite transformation in order to set up equilibrium between phases.

Risk about corrosion occurrence is susceptible when the sigma (Σ) phase forms in the zone of weld. They also exposed that the nitride generation and (delta (δ))-rich weld zone are caused by a high rate of cooling and loss for some extent of nitrogen (14). Higher heat input caused greater γ transition, intermetallic phase development, and larger grains sort of factors reduce corrosion resistance.

The HI conditions employed for the requisite better welded joint, meanwhile during examining a wide range of dissimilar weld joints (WJ) GTAW technology for assisting thermal and (NP P) nuclear power plants no reports of brittle failures has been discovered by researchers (15–19). Few researchers have tried to look at the dissimilar welded joints of DSS 2205 and SS304L, as per their literature review (20). The literature review unequivocally demonstrates that, to facilitate control production of harmful phases and optimize mechanical-metallurgical characteristics, the ideal HI for WJ of DSS 2205/SS304L is required as shown in table.1 hardness value has been improved after applying the TIG.

In order to improve structural integrity, the current is varied (150A to 195A) for achieving the dissimilar WJ in between DSS 2205 & SS304L by utilizing the GTAW technique with employment of ER2209 & ER309 filler. Previous studies also found increase in the tensile strength by applying high Heat input as shown in table 2.

Table 1: Shows Hardness Values in BM/WZ/HAZ

Author's	Hardness Value		Hardness Value Ha		Hardness	Hardness Value	Overall Impact on		
	Base metals (As received) in HV		Value in weld zone (Hv)	in Heat affected Zone (Hv)	Hardness				
	Plate-1	Plate-2							
(7)	(168) SS400	(198) SS304	446-514	200(SS400 side) & 200(SS 304 side)	Once the indenter travels from base zone to fusion zone from SS400 and SS304 side, then at boundaries value dipped to 338Hv and 257Hv				
(8)	(310) DSS2205	(200) ASS304	432	332(2205 side) & 292 (304 side)	Here ferrite formation pushes the hardness value improved about 23% and 32%, while using FLW in FZ part under Dss/Ass.				
(9)	200±11.5 (p92 steel)	195±10 (304H)	354±25	396±11(p92side)& 195±8(304Hside)	 Untempered martensite crystalline phase presence rise in hardness found. Absolute precipitation dissolution reason with alloying elements due 				

strengthening of solid solution in δ/γ matrix.

• δ-ferrite stringers agglomeration at ASS side of 304H in HAZ high value of hardness.

Table 2: Shows Observed	Tensile Strength in BM	/Post Weld Tensile S	Strength and Yield Strength

Author's	Tensile Strength Value Base metals (As received) in N/mm2 or MPa		Tensile Strength weldment (N/mm2)		Yield Strength of weldment (N/mm2)		•	
	Plate-1	Plate-2						
(10)	570(X70 steel)	800 (DSS2507)	724.6 309L	with	678.9 2594 fille	with r	SD2594 fabrication ductility tha	filler weld 11% rise in n filler 309
(11)	896 (2205)	783(304)	905		660(2205 329(304)	-	•	ve high strength cy values under 'S welding

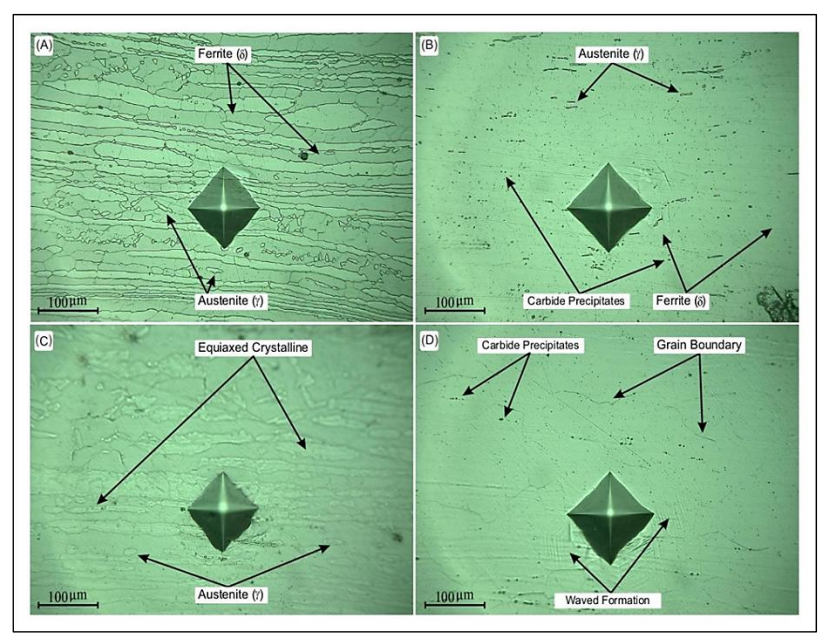


Figure 1: Optical Micro-Structure of BM (A) Duplex SS 2205/Filler 309L, (B) SS304L/Filler 309L, (C) DSS 2205/Filler 2209, (D) SS304L/Filler 2209

A thorough mechanical and metallurgical analysis of the WZ (weld zone), HAZ, and interface of weldment carried out. (SEM) Scanning electron microscopy and (OM) optical microscope were used to ensure integrity of the structure and properties. Thus, novelty of this study will provide a clear understanding of how suitable heat input combinations affect the metallurgical and mechanical performance for industrial application in order to attain the structural integrity of required dissimilar WJ.

Methodology

The basic materials employed in our investigation are SS304L & DSS 2205, which have dimensions of $125 \times 60 \times 10$ in mm. The gas tungsten arc welding (GTAW) joint is made from both base metals and duplex filler (ER2209 and ER 309l) with a 2.4 mm diameter. The base's nominal chemical composition has been listed in Table.3 with filler metals (FM). Figure 1 shows the base metal microstructure of DSS 2205 and SS304L. As we can observe in Figure 1(A-D), the microstructure of DSS2205 and SS304L is composed of austenite in

the medium of ferrite and at some extent carbide precipitates also prevailed.

The microstructure of DSS2205/SS304L base metal has been shown in given Figure. 1 (C and D),

it is composed of equiaxed gamma, with precipitates of carbides near grain boundary region.

Table 3: BM & FM Chemical Composition (wt %)

Used Material/											
Elements	Type	С	Mn	P	S	Mo	Cr	Ni	Cu	N	Si
DSS 2205	Base	0.03	2	0.03	0.02	3.5	23	6.5		0.2	1
SS 304L	Base	0.08	2	0.05	0.03		20	11			1
ER 309L	Filler	0.03	2.5	0.03	0.03	0.75	25	14	0.75		
ER 2209	Filler	0.03	2	0.03	0.03	3.5	23.5	9.5	0.75	0.2	0.9

Welding Parameter

The 125 x 60 x 10 mm base plates that were received were processed utilizing the wire cut electrical discharge machining process. Double V groove configurations (V-groove with root gap of 2 mm with 60° angle of bevel) are required as per (AWS) American Welding Society standard before welding (21). In order to achieve good weldability without any defects, the specimen was thereafter with help of acetone cleaned before taking them to welding in order to eradicate contamination (such as paint ,foreign particles, oxide scales, dirt, grease, etc.) along with penetrated metallic residue from surface. The burr was then carefully removed from the adjacent surface. In order to ensure proper alignment before welding, tacking was later performed at three different spots using the same filler. The **GTAW** multi-pass procedure was implemented using the root pass. At the termination of each weld pass, a SS wire brush was

quite handy to clean the weld zone and eliminate the inter-pass oxides, ensuring flawless weldment. Table .4 shows the HI measured for the DSS 2205/SS304L multi-pass weld as well as the parameter used for welding and certain other parameter with constant welding specification employed during experiment. These factors were taken into consideration when choosing heat input range for the current investigation, which were computed using analogous to currents: For greater heat input (HHI), we opted the corresponding values are 150 to 195 A (22, 23). The lower and higher HI arrangement were determined via the heat input equation, yielding 1.140 kiloJ/mm for High HI circumstances (arc efficiency kept at 60%) (24). The following formula was used to estimate the GTAW's heat input (25). Where V shows voltage, HI as the heat input, S shows welding speed, I show current, and η represents efficiency.

Heat Input =
$$\frac{\eta VI}{s}$$
 [1]

Table 4: Experimental Based Welding Parameters

			Heat Input	Welding Speed	Electrode
Pass	Voltage (V)	Current (A)	(kJ/mm)	(mm/min)	(mm)
Root	14	150	0.84	90	2.4
First Pass	16	195	1.40	90	2.4
Second Pa	ss 16	195	1.40	90	2.4
Cap Pass	16	195	1.32	90	2.4

Examination of Micro Structural Characteristics

In order to investigate the material characterization of the weldments, specimens measuring $55 \times 10 \times 10$ mm were machined using WCEDM. To achieve a (ultra-polished) mirror-like and without scratch surface, the metallographic processes were carried out compliant with ASTM E3-01 standard (26). After being manually

polished with help of emery paper (ranges from 220–2000 grit), the cross-sectioned specimens were disc polished using diamond paste of 1.5-lm. The microstructural characteristics of the weldment then revealed via etching the mirrorfinished samples (27). Using OM and SEM techniques, the microstructural properties of the WZ, BM, HAZ, and interface were examined. EDS qualitative analysis was used to characterize and determine the phase's chemical makeup.

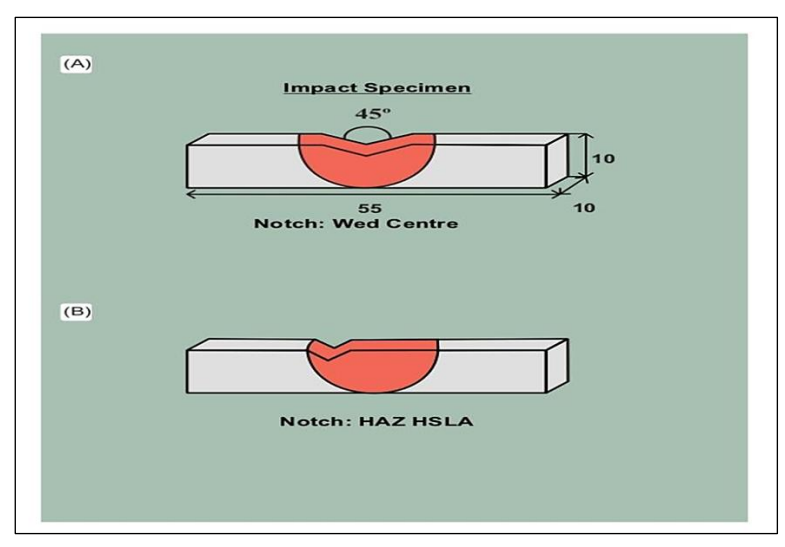


Figure 2: The Schematic Picture of (A) Impact Specimen (B) HAZ HSLA

Mechanical Characterization

Mechanical tests like impact, hardness, tensile testing was used to evaluate elements' joint reliability. WCEDM was used to construct the specimens in compliance with ASTM mechanical characterization criteria. The Vertical Tensile Testing Machine was used to conduct tests on the uniaxial tensile test coupons, which were manufactured in compliance with ASTM E8/E8M-21 requirements as shown in (Figure 2) (28). The cross-head speed used for the tensile testing was 0.15 mm/min. For the joint integrity of both weldments, tensile characteristics such as UTS, elongation, and 2% offset YS were measured. Crosswise specimens similar to those used in the metallographic examination were used to test the microhardness changes. A Vickers Micro hardness Tester was accustomed to taking readings the micro-hardness of the weldments, maintaining constant 0.25 mm gaps between them while applying a testing force of 0.5 kg-f and a dwell period of 10sec. To assess precise change in the hardness value, measurements were made across the WZ, HAZ, and BM of both weldments in accordance with ASTM E92-17 specification. According to the ASTM E23-12c specification, the impact toughness studies through Charpy V-notch of the WZ and HAZ of both weldments were conducted on a standard sub size specimen with a dimension of 55x10x10 mm (29). In order to assess the fracture mode and composition analysis of the precipitates, the broken impact/tensile specimens were inspected by means of a SEM accompanied with EDS. A few base metal tensile and impact specimens were also examined.

Results & Discussion Mode of Weld Solidification

The fraction of ferritic (delta) matrix in the weld is an important microstructure factor that is subjected to influence from chemical composition and heat exposure during multi-pass welding for improved impact toughness, hot cracking resistance, and corrosion (30). To determine the weldability of the dissimilar joints of DSS 2205/SS 304L, the Schaeffer diagram can be used to compare and validate the results. The ferritoscope measurement can theoretically be used to estimate the fair ferrite number to determine ferrite content of weldment. Hypothetically, the Schaeffer diagram may determine the ferritic (delta) phase amalgamation of weld and forecast the solidification mode of weld and transition zones. According to the weld chemistry, Table 5 lists the Chromium (Cr) and (Nickel) Ni equivalent of the ER2209 & ER309L weldment for High HI circumstances along with its solidification mode. For Filler ER2209 and ER309L HHI settings, the Creq/Nieq ratios are 1.59 and 2.48, respectively. The Schaefer diagram is very useful for predicting the final deposit structure of weld metals.

Table 5: Creq & Nieq Values of Both Fillers

Filler Material	Type	Cr_{eq}	Nieq	Cr_{eq}/Ni_{eq}	Solidification Mode
309 L	Filler	25.75	16.15	1.59	Ferrite-Austenite
2209	Filler	28.35	11.4	2.48	Ferrite

Widmanstatten austenite (WA), intergranular austenite-gamma (IGA), and grain boundary austenite-gamma (GBA) undergo solid phase transformation after primary ferrite solidification (31-33). Achieving a balanced relationship between mechanical and corrosion properties requires optimizing the ferrite infusion in the WZ. The primary cause of aforementioned observation is the impact of HI on the pace of cooling and the amount of time needed for delta to change into gamma. Because there is sufficient transformation with higher HI, a lower rate of cooling results in lower ferrite content. While high ferrite content (greater than 75 percentage points) might diminish impact toughness and corrosion resistance qualities, low ferrite content (less than 25 percentage points) can cause mechanical strength to deteriorate (34, 35). Consequently, the ferrite infusion of the weld zones increases as the HI increases. With rise in HI, a notable increase in (RA) reformed austenite (i.e WA, GBA, and IGA) inside the ferrite constituency has been visualize. More ferrite to austenite transition is caused by postponing cooling, which lengthens transformation time and allows for the cstabilizing elements diffusion in great quantity (i.e. N and Ni).

Weld Region Micro-structural Effect

During High HI weldment begin root to cap pass, the micro-structural changes observation for ER2209 and ER309L filler in the WZ vicinity shows a diverse microstructure made up of delta phase and RA. Figure 3 (A-D) and Figure 4 (A-D) display the High HI weldment microstructure begin from root till end known as cap pass, respectively. For both HI circumstances, partially converted austenite (PTA), GBA, WA, IGA are the most notable microstructure characteristics. But on the micrograph, with gamma appearing as intragranular precipitates or WA intercept crosswise to long axis, the presence of GBA and WA is plainly obvious. It is crucial to remember that during welding, the arc must be sufficient to produce a respectable amount of austenite production in the WZ and HAZ. To reach the finest possible structural superiority of the weldment with enhanced mechanical and corrosion properties, minimum amount of gamma in the root and cap passes should be between 30 and 70 percent (36, 37). More ferrite turns into austenite when the heat input is increased because under high temperature weld specimen is unravel for longer periods with a slower rate of cooling. During WZ root to cap pass investigation heating cycle because precipitation of numerous austenite morphologies observed. As heat input increased, the RA microstructure evolution in the weld zone progressively shifted from GBA and Reformed Austenite to IGA and WA respectively. After cooling, the GBA, which was initially nucleated from bigger untransformed austenite, takes on a jagged aspect (38, 39).WA is another common RA morphology that forms as cooling proceeds. Further WA nucleates and develops at the ferrite grain (FG) borders, within the FG, or at the GBA and ferrite phase contour along with skeletal dendritic formation found there. At lower temperatures than GBA, WA merges as the needle-like edge and grows as long, straight lathe plates. The partially transformed austenite (PTA), which looks like the ferrite slices WA, is diamond-shaped, ordered, and degraded from WA. The longer cooling time caused by the increase in heat input results in a longer time for WA creation, and at high temperatures, WA loses its stability to disintegrate. Grain development in the weld zone is restricted by PTAs (40, 41). It has been visualize from Figure 3(A-D) and 4(A-D), IGA is discrete throughout the FG and exhibits smaller morphology other than Grain BA and WA because it needs less driving push and got some addition time to grow. As a result, it dominates the final microstructure. Consequently, compared to IGA, GBA and WA may manifest at greater temperatures and with less under-cooling (42, 43). As seen in Figure 5 (A-D), the WZ microstructural observation also demonstrates creation of the no mixed zone (NMZ) resembling an island in high HI. The liquidus temperature differential between the base metal and filler causes the UZ that comes into direct contact with the weld metal to create many small islands in Figure 5 (B).

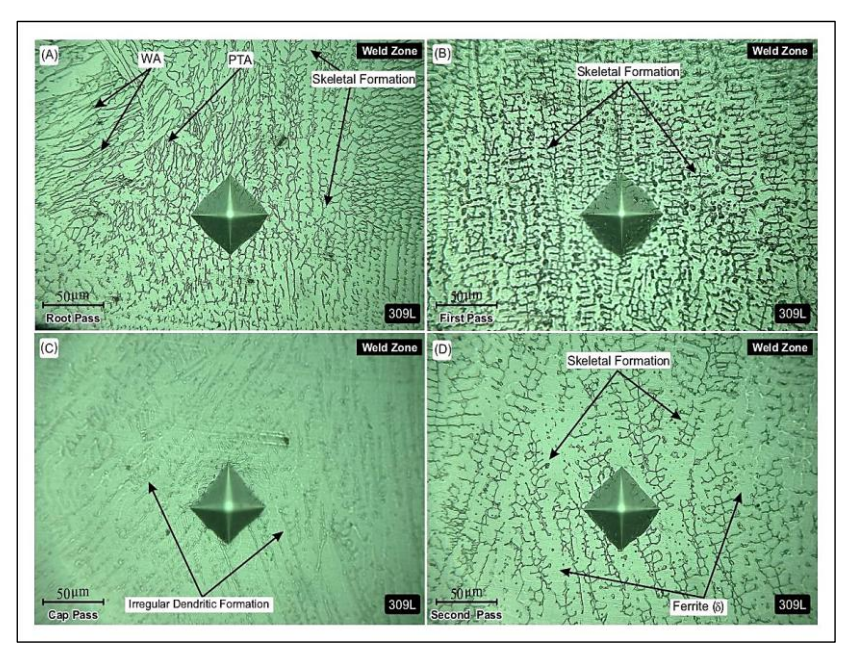


Figure 3: WZ Microstructure Evolution of HHI of Filler 309L Weldments Representing (A) Root pass WA, Skeletal Formation, PTA and Ferrite (B) First Pass (C) Cap Pass (D) Second Pass

The characteristic of elements macro segregation along the borders, which results in multiple boundary (i.e boundary 1 and 2) phenomena and changes in the rate of solidification due to the expansion of temperature gradient and their impact over the solidified micro-structure, is depicted in Figure 5(C and D). The boundary formation and island creation in the weld zone have also been documented by other researchers (44, 45). The two successive passes' varying growth rates (R),cooling rates, and temperature

gradients (G) are what cause the variation in microstructural changes from pass begin from the root to cap. In the cap pass of 309L HHI weldment, structure with columnar dendritic (skeletal) morphology would result from a decrease in cooling rate brought on by the subsequent of filling passes and the welding HI impact, as shown in Figure 5A. numerous researchers have found that compared to primary austenite, $\gamma 2$ deteriorates the pitting corrosion resistance more (46, 47).

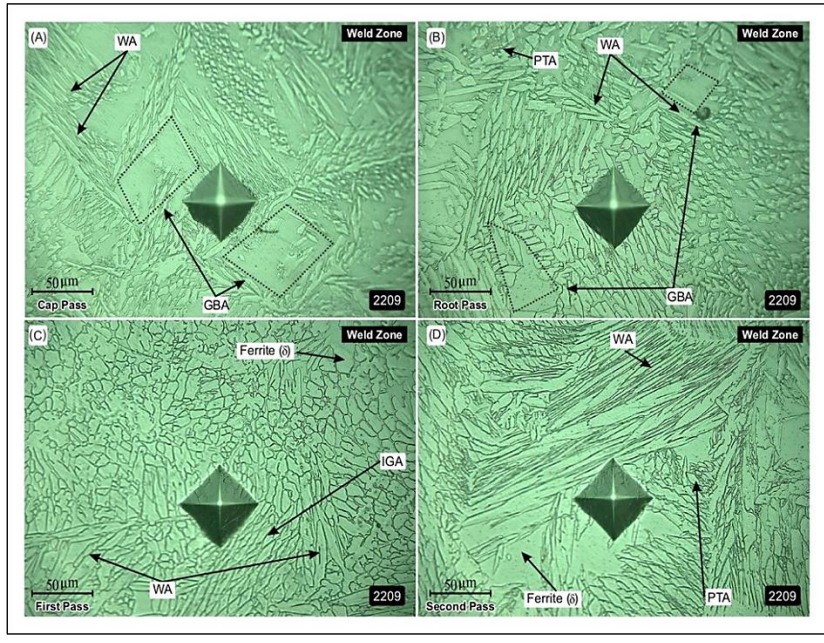


Figure 4: WZ Microstructure Evolution of HHI of Filler 2209 Weldments Representing WA, GBA, PTA and Ferrite in (A) Cap (B) root (C) First and (D) Second Passes

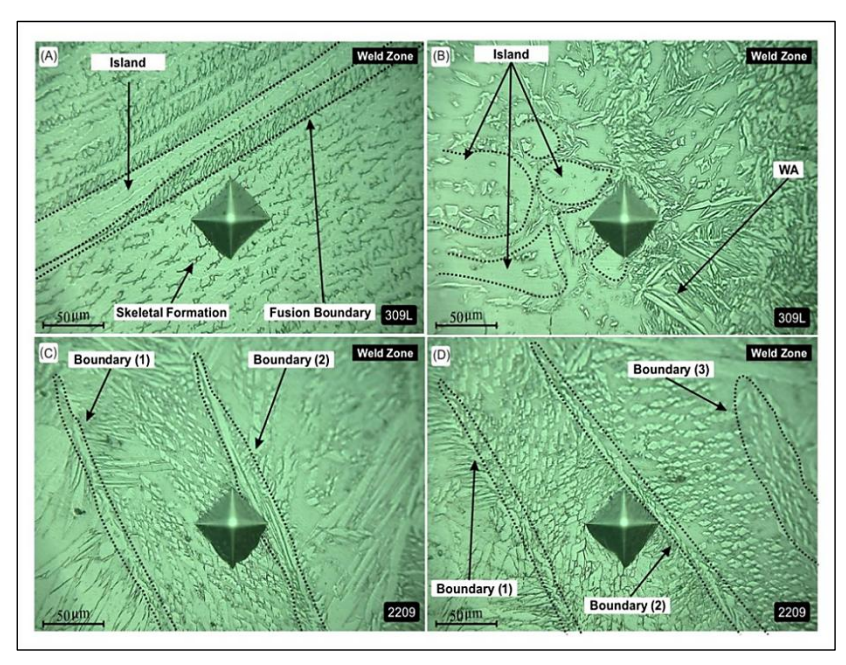


Figure 5: (A-D) WZ Islands and Boundary Formation of Filler 309L/2209

Heat Affected Region Micro-Structural Effect

Variations in heat input during welding have an impact over mechanical characteristics and microstructure development of DSS2205/SS304L weldments, making them a crucial parameter. Thermal cycles pushed greater influence on the micro-structural changes of the HAZ than BM & FM welding and chemical makeup. The evolution of the microstructure shows that HI rise causes the HAZ width and grain size to increase close to the fusion boundary and weld contact.

The same has been documented by other researches (48, 49). The fusion boundary, weld zone, and HAZ microstructure evolution are depicted in the optical micrographs for HHI in Figures 6[A-D]. The SS304L side's HAZ is rather small under both heat input scenarios. While comparing the WZ, the (RA) reformed austenite development in the HeatAZ is suppressed by a higher cooling rate and more heat cycles. The DSS 2205 side's interface and HAZ microstructure for HHI employing ER2209/ER 309L filler can be observed in Figure 6 (B and C). The ferrite matrix's γ grain network makes up both HAZ zones. With a thermal cycle, the HTHAZ is situated close to the fusion boundary. When heated, the HTHAZ microstructure became nearly entirely ferritic. Additionally, the LTHAZ is a region next to HTHAZ and distant from the fusion barrier where the ferrite-austenite balance cannot be significantly changed by the heat cycle (50). Typically, during

the many passes of welding or continuous reheating, Heat-AZ under metastable state may ensue austenite precipitation. An essentially complete ferrite structure will emerge at high temperatures as a result of the change of δ to γ occurring as the HAZ temperature increases following the application of many passes. The SE micrograph of the DSS2205 interface and HAZ close to the fusion border is displayed at varying magnification for HHI conditions, in Figure 6(B-C). There is coarsened grain development of ferrite (delta) close to the fusion border because the high cooling rate will not provide sufficient duration for gamma to nucleate and cultivate from delta. As seen in Figure 6(B) the primary morphological nucleates close to the DSS 2205 HAZ are GBA, WA, and IGA, columnar dendrites dispersed throughout the ferrite structure matrix. Rapid cooling of the HAZ from peak to atmospheric temperature results in a variety of reformed austenite morphological forms. Furthermore, the quantity of reformed austenite phases and the morphological shift from GBA to WA and IGA seem to have been somewhat impacted by heat input. As a result, ferrite grain development took place without a significant number of intermetallic phases. The BM was maintained above the delta solvus for a longer period of time by multipass welding, which advanced this grain development. Therefore, as Figure 6(B) and (C) demonstrate, PTA, GBA and trace quantities of WA only which may develop in the HTHAZ after cooling.

The HAZ and interface region of the micrograph are composed of carbide precipitation and deltaferrite with ferrite stringer. Due to the heat cycles involved in multi-pass, primary ferrite and secondary austenite precipitate, sinking the likelihood of hot cracking breakdown in the Heat AZ. Figure 7(A-D) shows EDS spectra for HAZ corresponding to HHI Interface. Spectrum 3 shows high Cr, Ni content while Spectrum 26, 5 and 14 exhibit comparative low Cr and Ni precipitation. The Line mapping study of the HHI is shown in Figures 8 (A-F) and 9(A-F). During mapping of the main alloying constituents (i.e., Mn, Fe, Silicon, Ni, Mo, and Cr), HHI weldment was achieved in the HAZ, weld zone, and base metal zones. Since the light element character creates ambiguity throughout the HAZ in the elemental analysis, carbon is excluded during the line mapping. For all heat input circumstances, the EDS spectra demonstrate notable gradient fluctuation of Fe, Cr,

and Mn segregation as we traverse the DSS 2205 to SS304L. The elemental line mapping analysis of the HHI weldments over SS304L BM/WM interface is shown in Figure 8(A-B) and Figure 9(A-B), respectively. This confirms the modest migration of elements due to the comparable chemical composition of ER 2209/ER 309L filler and SS304L metal. The EDS/SEM investigation substantiate the little migration of elements (i.e., Mo, Silicon, Mn, Nickel and Cr) from Heat-AZ to WZ, which is covered in the microstructure development of HAZ Conversely, High HI weldment elemental line mapping study over the DSS2205 and SS304L shows in contrast to the Ni and Mn components, the data indicate that the Cr has stirred from the weld to the SS304L Heat-AZ. mapping observation and line microstructure examination of the Heat-AZ show that the weld interface of High HI has higher Fe and Cr.

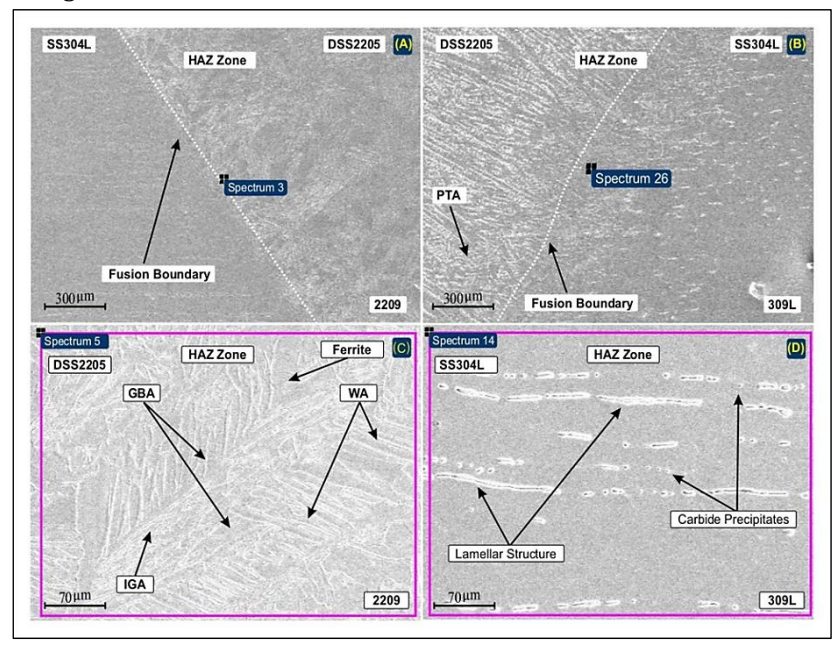


Figure 6: Microstructure Interpretation of ER309L/2209 with BM for HHI Weld (A and C) HAZ Interface for 304L/2205 Corresponding to ER2209 (B and D) HAZ Interface for 2205/304 Corresponding to ER309L

Analysis of Micro-hardness

In HHI, the micro-hardness profile is present throughout the welded joints of DSS 2205/SS304L. For both heat input settings, the specimen's microhardness was measured longitudinally (the interface and weld) and transversely (cap pass towards root pass). At regular intervals twenty indents were made from the centre of weld arena to BM on both sides, with center of weld arena serving as reference point (X equals to zero). The

hardness values for SS304L and DSS 2205 base metal measurements are 201Hv0.5 and 293Hv0.5, respectively. The analysis of micro-hardness reveals that there are slight differences in the HAZ's hardness value for the two filler 309L/2209 inputs circumstances. The 309L HAZ micro-hardness rises from 203.63Hv0.5 to 281.91Hv0.5 as the indenter moves horizontal from the weld zone towards HAZ; similarly 2209 filler micro-hardness rises from 246.72Hv0.5 to 283.94Hv0.5

horizontally from WZ to HAZ. While by rising HI the grain coarsening tends to grow, as observed in the HAZ optical micrograph as shown in Figure 6(A-D). The ratio of austenite to ferrite, the carbide distribution distinction and its shape, any secondary phases arising from the weld zone, and the variance in Cr concentration in Heat-AZ DSS 2205 are some of the crucial factors that might influence the hardness. Furthermore, the hardness increase between the fusion boundary and the columnar dendrites for both HI validates the development of micro-constituents in the SS304L side's Heat-AZ.

The microstructure evolution of the weld zone (Figure 4 and 5) describes a number of significant factors that contribute to the decrease in hardness value from 2209 to 309L HHI. These factors include rate of cooling, the ratio of gamma to delta, the lower ferrite content, the precipitation presence or absence, and the coarse grain

structure. The change in hardness value might be influenced by a numerous factors, including the amount of ferrite phase there in the weld zone. First, a quicker cooling rate results from the production of tiny ferrite grains due to reduced heat input, which restricts the growth of ferrite grains. Second, when heat input rises, the value of hardness dropped due to the development and nucleation of reformed austenite. The value of hardness from C to R in the WZ, HHI ranges from around 245.02Hv0.5 to 305.59Hv0.5 on average. As the indenter moves from cap to root, the value for hardness slowly lessen due to changes in HI and cooling rate. The simultaneous cooling and heating process that takes place during multi-pass welding, as well as the fluctuating HI throughout each pass, may be the reason of this non-uniform micro-hardness vacillation along the fusion zone in weld arena.

Table 6: Stress-Strain Values for 309L and 2209 Fillers

Filler	Max Force at entire area in N	Max Stress at entire area in N/mm2	Max Strain at entire area in %
2209	27389.8	624.447	55.8245
309L	27052.0	624.613	54.5846

Evaluation of Tensile Test

Based on the transverse tensile tests conducted at room temperature for BM and WJ under High-HI circumstances utilizing ER2209 and ER309L filler, the conclusion may be drawn as per SS graphs.

The stress-strain charts are exhibit in Figure 10(A-B), and Table 6 presents the data that were obtained. To enhance and comprehend the mechanical characteristics of the (WJ), which are significantly impacted by welding settings, it is imperative to investigate the fracture site. Here we found max force at entire area is 27389.8 N & 27052.0 N for 2209 and 309L filler respectively, also the max. Tensile strength reported 624.447 N/mm² & 624.613 N/mm² for fillers 2209 and 309L respectively (Table 6) the both weldments following the fracture. For HHI, the fracture takes place near WZ. However, the HHI test specimens had a greater average tensile strength than the DSS 2205 base metal, despite breaking from the weld center. According to these findings, there is no discernible indication of ductility or plastic deformation, and the welded joints shatter under conditions of local and heterogeneous deformation.

Impact Test

According to the standard specification, the Charpy impact toughness (CIT) test was carried out at RT to find out the toughness performance of the BM, Heat-AZ, and WZ under the rapid weight of impact for both HI weldments of DSS 2205/SS304L. The specimen was shaped using Wire-CEDM, and the Vnotch was formed on the BM, the Heat-AZ of both sides, and the WZ for High-HI weldment. After the CIT test, it was also observed that the fracture was in ductile mode and that the fractured sample weren't entirely alienated, displaying V-notch bend SEM examined BM fractured samples, and Figure 11 (A-B) displays the fractograph. The ductile mode of fracture is demonstrated by the Scanning-EM fractograph of both BM, which includes ductile tearing ridges, micro voids dimple coalescence, facets, cleavage facets, and parabolic dimples. Sufficient quantity of phase transition from ferrite to RA may enhance weldment's toughness, which in turn raises the impact energy (51).

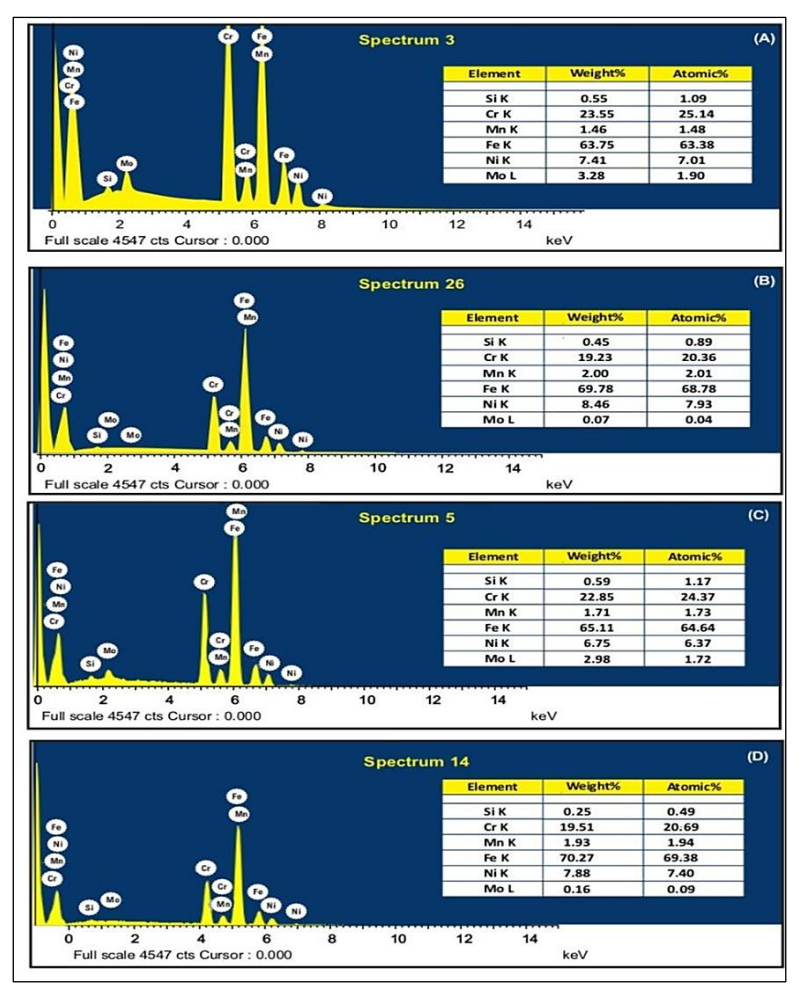


Figure 7: EDS Spectra for HHI Interface using ER309L/2209 for DSS2205 and SS304L

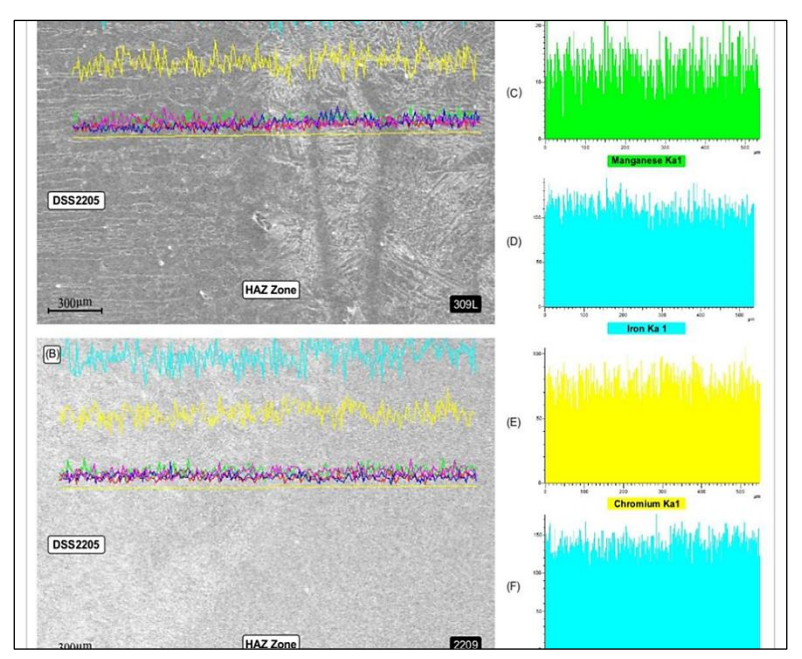


Figure 8: Line Mapping Elemental Investigation on the High-HI with Filler ER309L/ER2209 (A-B) DSS2205 HAZ (C-F) Elements Distribution in Region

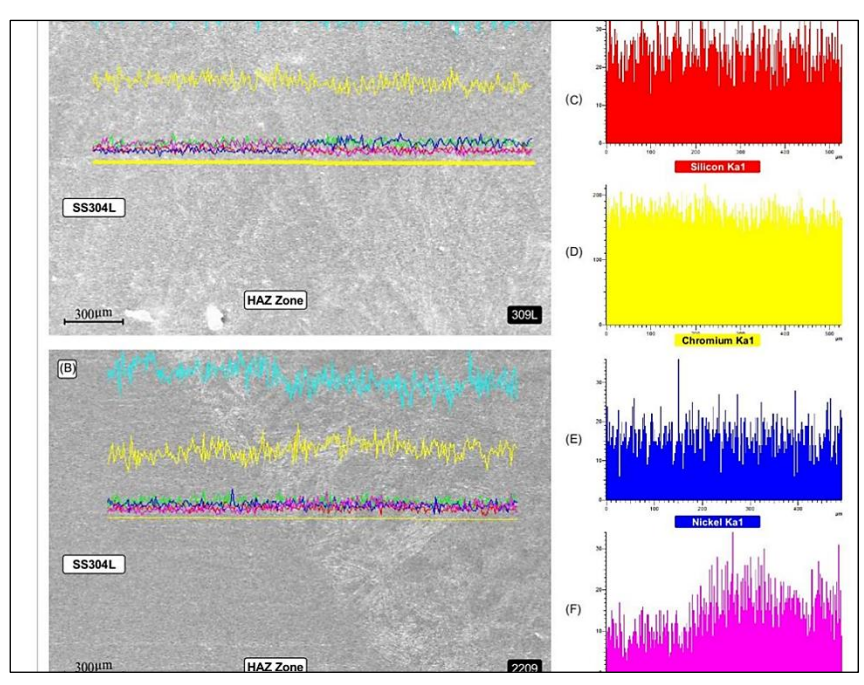


Figure 9: Line Mapping Elemental Analysis on the HHI using Filler ER309L/ER2209 (A-B) SS304LHAZ (C-F) Elements Distribution in Region

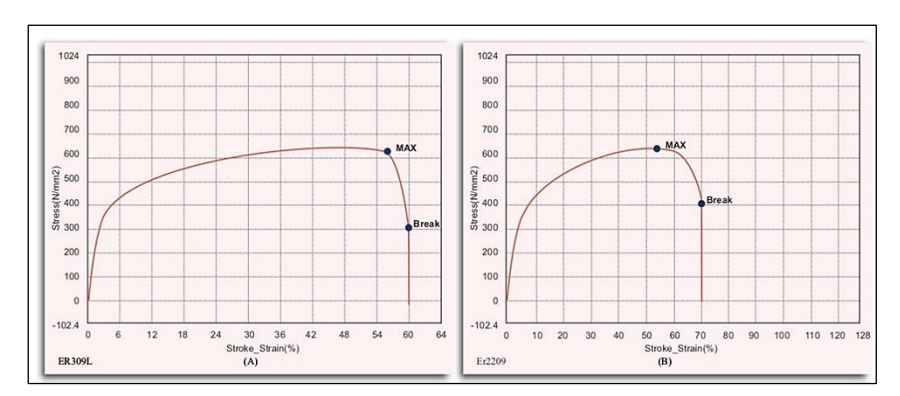


Figure 10: Strain Graph for (A) Filler ER309L (B) Filler ER2209

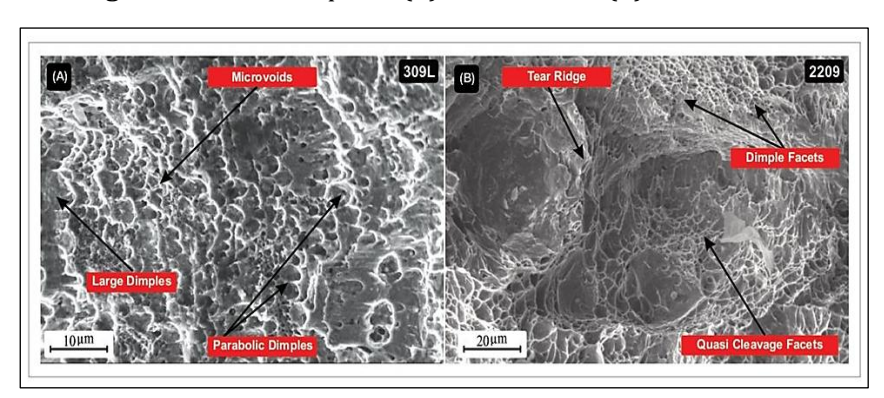


Figure 11: SEM Fractograph for HAZ Weldments for DSS2205/SS304L (A) for Filler ER309L (B) for Filler ER2209

The company of secondary phases, for instance secondary austenite and sigma phases is another important element that affects impact toughness (52-53). The most frequent fracture mechanism in impact testing, as shown by these fractographs, is ductile failure. This specific fracture process is

characterized by the pattern of dimples on the fractured surface.

In the non-homogeneous plastic deformation zone, an austenitic alloy causes many dimples or kind of voids to appear on the fractured surface. Impact toughness is influenced by heat input on the

formation of HAZ microstructural features. The HAZ is made up of sub-critical and inter critical heating zones as well as fine and coarse grain areas. On the fractographic surface, it frequently displayed inclusion particles, ductile tearing ridges, dimples, micro voids and ductile facets. It is evident from Figure 11 that the austenite phase is linked to dimple, while ferrite is linked to quasicleavage fractures. Due to river and sand mole that develop along the fracto-graphic region under High-HI conditions for both HAZ.

Conclusion

This study used ER 2209 and ER309L filler at elevated heat inputs to inspect the cause of welding HI on the quality of weld for DSS2205 and SS304L weldments by utilizing the GTAW technique. The mechanical characteristics and microstructure evolution of HHI weldments were thoroughly examined and described. The study's evaluations yielded the many significant finding, Solid-state transformation leads to a wide range of microstructure evolution, and the GTAW process convinces solidification through weldments. Nonetheless, the microstructure of both weldments was nearly identical and included a number of reformed austenites, including (IGA) precipitates inside the ferrite surrounding substance, Widmanstatten austenite (WA), and boundaries austenite (GBA). precipitation of RA occurs in a chronological order, which has a substantial influence over the structural reliability of both HI weldments. HI has notable influence on the fusion boundary and HAZ area. Noteworthy growth of grains and the degree of grain coarsening are observed in every Heat-AZ of both weldments as heat input increases. In both 3091/2209 weldments, the epitaxial growth took place at the DSS 2205 contacts. A significant difference in the δ - γ phase balance between the Heat-AZ and WZ compared to BM is observed when the HAZ contains a high ferrite percentage. According to the mechanical evaluations, there is no discernible change in hardness when heat input is present. Nevertheless, the hardness decreases with increasing heat input, which might be ascribed to the different δ/γ ratios in the HAZ and the WZ. According to micro-hardness investigation, the two filler 309L/2209 input conditions have somewhat different HAZ hardness values .As the indenter goes horizontally from the WZ towards HAZ, 309L HAZ micro-hardness increases from 203.63 Hv 0.5 to 281.91 Hv 0.5; likewise, the 2209 filler micro-hardness increases from 246.72 Hv 0.5 to 283.94 Hv 0.5 horizontally from WZ to HAZ. For 309L and 2209 filler, the HHI weldments' tensile strength parameter, or maximum force, was 27052N and 27389.8N, respectively. The ductility mode of fracture is visible for every trail in the fractography of both weldments. The toughness value was found to have decreased more significantly in the ASS304 HAZ notched specimens due to secondary phase development. The fractographs of the samples demonstrated that for all BM, WZ, and Heat-AZ specimens, ductile mode fracture is predominant. According to the current investigation, the composition of both fillers at high heat input has nearly identical advantageous characteristics to achieve the structural integrity of the welds of DSS2205/SS304L DWJ utilizing ER 2209 and ER 309L fillers. However, more research on LHI is advised with the intention of gain a better knowledge of the impact toughness of weldment.

Limitations & Future Scope

We have study many aspects of the DMW joints in this section. However detailed failure analysis, impact energy, corrosion resistance, intermetallic compounds analysis, XRD/EBSD analysis has not been discussed in this study. Hence for future research, we can investigate the processes of in mixed joints, particularly concentrating on specific environmental factors. Gaining insights into the elements that lead to corrosion, like the interplay between various phases and chemical compositions, could inform the creation of welding methods that resist Additional developments corrosion. microstructural analysis (Fracture surface, XRD etc) methods could be investigated, including sophisticated microscopy or in-situ characterization approaches. These methods have the potential to offer more comprehensive insights into the progression of phases, grain structures, and defects that occur during welding, enhancing our understanding of material behavior.

Abbreviations

GBA: Grain Boundary austenite, HHI: High Heat Input, HTHAZ: High Temperature Heat affected zone, IGA: Inter Granular austenite, LHI: Low heat input, LTHAZ-Low Temperature heat affected

zone, PTA: Partially Transformed Austenite, RA: Reformed Austenite, WA: Widmanstatten austenite, WJ: Weld Joints.

Acknowledgement

The authors would like to recognize the carrying out tests support imparted by Dr. Anup Maurya, IIT Jodhpur.

Author Contributions

Gyanendu Sharma: Conceptualization, Methodology, Investigation, Formal analysis, Writing-original draft, Writing - review & editing, Bhupendra Singh Chauhan: Conceptualization, Methodology, Project administration, Writingreview & editing.

Conflict of Interest

The authors affirm that none of the work described in this publication may have been influenced by any known contending monetary interests or ties.

Declaration of Artificial Intelligence (AI) Assistance

Not Applicable.

Ethics Approval

Not Applicable.

Funding

Not Applicable.

References

- Zhang T, Wang W, Zhou J, et al. Interfacial characteristics and nano-mechanical properties of dissimilar 304 austenitic stainless steel/AZ31B Mg alloy welding joint. J Manufac Proc. 2019;42:257-65.
- 2. Maurya A.K, Pandey C, Chhibber R. Dissimilar welding of duplex stainless steel with Ni alloys: A review. Int J Press Vessel
 Pip. 2021;192:104439. http://dx.doi.org/10.1016
 /j.ijpvp.2021.104439
- 3. Labanowski J, Fydrych D, Rogalski G, et al. Underwater welding of duplex stainless steel. Solid State Phenom. 2012;183:101–6.
- Gunn R, editor. Duplex stainless steels: Microstructure, properties and applications. Elsevier, Cambridge; 1997. https://api.semanticscholar.org/CorpusID:13761 6149
- Nissley N, Anderson TD, Noecker FF, et al. Dissimilar metal welding of nitronic 50 HS and 25% Cr super duplex stainless steel. Proc Int Conf Offshore Mech Arct Eng - OMAE, ASME.

2014;5.

https://doi.org/10.1115/OMAE2014-24706

- 6. Muthupandi V, Bala Srinivasan P, Seshadri S.K, et al. Effect of weld metal chemistry and heat input on the structure and properties of duplex stainless steel welds. Mater Sci Eng A. 2003:358:9–16.
- 7. Chen HC, Ng FL, Zheng LD. Hybrid laser-TIG welding of dissimilar ferrous steels:10 mm thick low carbon steel to 304 austenitic stainless steel. J Manufac Proc. 2019;47:324–36.
- 8. Mohammed GR, Ishak M, Syed Ahmad SNA, et al. Fiber laser welding of dissimilar 2205/304 stainless steel plates. Metals. 2017;7:546. https://www.mdpi.com/2075-4701/7/12/546
- Sharma P, Dwivedi DK. A-TIG welding of dissimilar P92 steel and 304H austenitic stainless steel: Mechanisms, microstructure and mechanical properties. J Manufac Proc. 2019;44:166-78.
- Khan WN, Chhibber R. Effect of filler metal on solidification, microstructure and mechanical properties of dissimilar super duplex/pipeline steel GTA weld. Mater Sci Eng A. 2021;803:140476.
 - https://www.sciencedirect.com/science/article/abs/pii/S0921509320315392
- 11. Wang W, Hu Y, Zhang M, et al. Microstructure and mechanical properties of dissimilar friction stir welds in austenitic-duplex stainless steels. Mater Sci Eng A. 2020;787:139499. doi: 10.1016/j.msea.2020.139499.
- 12. Yousefieh M, Shamanian M, Saatchi A. Influence of heat input in pulsed current GTAW process on microstructure and corrosion resistance of duplex stainless steel welds. J Iron Steel Res Int. 2011;18:65–9.
- 13. Yousefieh M, Shamanian M, Saatchi A .Optimization of the pulsed current gas tungsten arc welding (PCGTAW) parameters for corrosion resistance of super duplex stainless steel (UNS S32760) welds using the Taguchi method. J Alloys Compd. 2011;509:782–8.
- 14. Hosseini VA, Hurtig K, Karlsson L. Effect of multipass TIG welding on the corrosion resistance and microstructure of a super duplex stainless steel. Mater Corros. 2017;68:405–15.
- 15. Sirohi S, Kumar A, Soni S, et al. Influence of PWHT parameters on the mechanical properties and microstructural behavior of multi-pass GTAW joints of P92 steel. Materials. 2022;15:40-5.
- Rogalski GA, Świerczyńska A, Landowski M, et al. Mechanical and microstructural characterization of TIG welded dissimilar joints between 304L austenitic stainless steel and Incoloy 800HT nickel alloy. Metals. 2020;10:559. https://scispace.com/papers/mechanical-and-

- microstructural-characterization-of-tig-hq5owv4uho
- 17. Sharma AK, Fydrych D, Sirohi, A, et al. Study on microstructural characterization, mechanical properties and residual stress of GTAW dissimilar joints of p91 and p22 steels. Materials. 2021;14:65-91.
- 18. Sabzi M, Mousavi Anijdan SHM, Eivani AR, et al. The effect of pulse current changes in PCGTAW on microstructural evolution, drastic improvement in mechanical properties, and fracture mode of dissimilar welded joint of AISI 316LAISI 310S stainless steels. Mater Sci Eng A. 2021;823:141700.
 - https://www.sciencedirect.com/science/article/pi i/S0921509321009680
- 19. Reza T, Sabzi M, Anijdan SH, et al. Comparing the effect of continuous and pulsed current in the GTAW process of AISI 316L stainless steel welded joint: Microstructural evolution, phase equilibrium, mechanical properties and fracture mode. J Market Res. 2021;15:199–212.
- 20. Maurya AK, Pandey C, Chhibber R. Effect of filler metal composition on microstructural and mechanical characterization of dissimilar welded joint of nitronic steel and super duplex stainless steel. Arch Civil Mech Eng. 2022;22:1–28.
- 21. AWS D. Structural welding code-Steel. Mar Lin; 1978. https://blog.ansi.org/ansi/aws-d1-1-2025-structural-welding-code-steel/
- 22. Kumar GS, Ramesh M, Dinesh S, et al. Investiga tion of the TIG welding process for joining AA6082 alloy using grey relational analysis. Adv Mater Sci Eng. 2022:1–8. https://doi.org/10.1155/2022/5670172
- 23. Karthick K, Sravanthi K, Jani SP, et al. Optimization of TIG welding parameters and filler rod material selection for dissimilar aluminum alloy joints. J Mater Sci: Mater Eng. 2025;20:80. https://doi.org/10.1186/s40712-025-00296-7
- 24. DuPont JN, Marder AR. Thermal efficiency of arc welding processes. Weld J Includ Weld Res Suppl. 1995;74:12. https://www.osti.gov/biblio/170250
- Ahmed N, editor. New developments in advanced welding. Elsevier; 2005. https://shop.elsevier.com/books/new-developments-in-advanced-welding/ahmed/978-1-85573-970-3
- 26. Marcondes F. Standard guide for preparation of metallographic specimens 1, ASTM Inter. 2012;3(1):1–12. https://www.studocu.com/co/document/fundacion-de-estudios-tecnicos/informatica/astm-e3-112017-standard-guide-for-preparation-of-metallographic-specimens/39218120
- 27. Practice S. Standard practice for microetching metals and alloys ASTM E-407. 2016;7:1–22. https://store.astm.org/e0407-07r15.html

- 28. Standard Test Methods for Tension Testing of Metallic Materials. Annual Book of ASTM Standards.2010;4:1–28. https://www.galvanizeit.com/uploads/AS TM-E-8-yr-13.pdf
- Standard test methods for notched bar impact testing of metallic materials. ASTM International. 2012.
 https://www.scribd.com/document/709583603/A STM-E23-Impact-Testing-2012-Standard-1
- 30. Vahman M, Shamanian M, Golozar MA, et al. The effect of welding heat input on the structure-property relationship of a new grade super duplex stainless steel. Steel Res Int. 2020;91:1-12.
- 31. Liu Y, Mao E, Xu L, et al. Research of the formation mechanism of widmanstatten ferrite in 30 Mn2 steel in emerging computation and information technologies for education. Adv Intell Soft Comput. 2012;146:695-9.
- 32. Cao S, Wu S, Zhang C, et al. Three-dimensional morphology and analysis of Widmanstätten sideplates ferrite. Metals. 2022;12(3):523. https://www.mdpi.com/2075-4701/12/3/523
- Gao Z, Hu R, Gao X, et al. Characterization of the Widmanstätten structure in γ-TiAl alloy using an EBSD-FIB-TEM combined process. Scripta Materialia. 2023;222:115001. https://www.sciencedirect.com/science/article/pi i/S1359646222004961
- 34. Rahmani M, Eghlimi A, Shamanian M. Evaluation of microstructure and mechanical properties in dissimilar austenitic/super duplex stainless steel joint. J Mater Eng Perform. 2014;23:3745–53.
- 35. Gupta A, Kumar T, Baskaran SB, et al. Effect of heat input on microstructure and corrosion behavior of duplex stainless steel shielded metal arc welds. Trans Indian Inst Met. 2018;71:1595–1606.
- 36. Ouali N, Khenfer K, Belkessa B, et al. Effect of heat input on microstructure, residual stress, and corrosion resistance of UNS 32101 lean duplex stainless steel weld joints. J Mater Eng Perform. 2019;28:4252–64.
- 37. Sadeghian M, Shamanian M, Shafyei A. Effect of heat input on microstructure and mechanical properties of dissimilar joints between super duplex stainless steel and high strength low alloy steel. Mater Des. 2014;60:678–84.
- 38. Ramirez AJ, Lippold JC, Brandi SD. The relationship between chromium nitride and secondary austenite precipitation in duplex stainless steels. Metall Mater Trans A. 2003;34:1575–97.
- 39. Eghlimi A, Shamanian M, Eskandarian M, et al. Evaluation of microstructure and texture across the welded interface of super duplex stainless steel and high strength low alloy steel. Surf Coat Technol. 2015;264:150–62.

- 40. Khan WN, Mahajan S, Chhibber R. Investigations on Reformed Austenite in the Microstructure of Dissimilar Super Duplex/Pipeline Steel Weld. Mater Lett. 2021;285:129109. https://www.sciencedirect.com/science/article/pii/S0167577X20318164
- 41. Ohmori Y, Nakai K, Ohtsubo H, et al. Mechanism of Widmanstätten austenite formation in a δ/γ duplex phase stainless steel. ISIJ Int. 1995;35(8):969-75.
- 42. García-Mateo C, Caballero FG. The role of retained austenite on tensile properties of steels with bainitic microstructures. Mater Transac. 2005;46(8):1839-46.
- 43. Sieurin H, Sandström R. Austenite reformation in the heat-affected zone of duplex stainless steel 2205. Mater Sci Eng A. 2006;418(1-2):250-6.
- 44. Kumar S, Pandey C, Goyal A. A microstructural and mechanical behavior study of heterogeneous P91 welded joint. Int J Press Vessels Pip. 2020;185:104-28.
- 45. Dak G, Pandey C. A critical review on dissimilar welds joint between martensitic and austenitic steel for power plant application. J Manufac Process. 2020;58:377–406.
- 46. Zhang Z, Jing H, Xu L, et al. Influence of heat input in electron beam process on microstructure and properties of duplex stainless steel welded interface. Appl Surf Sci. 2018;435:352–66.
- 47. Nilsson JO. Super duplex stainless steels. Mater Sci Technol. 1992;8(8):685-700. doi: 10.1179/mst.1992.8.8.685.

- 48. Kumar S, Shahi AS. Effect of heat input on the microstructure and mechanical properties of gas tungsten arc welded AISI 304 stainless steel joints. Mater Des. 2011;32:3617–23.
- 49. Yang Y, Yan B, Li J, et al. The effect of large heat input on the microstructure and corrosion behaviour of simulated heat affected zone in 2205 duplex stainless steel. Corros Sci. 2011;53:3756–63.
- 50. Westin EM, Wessman S. Characteristics of hightemperature heat-affected zones in duplex stainless steels. Weld World. 2024;68(8):1981-97.
- 51. Garcia-Garcia V. Microstructural and mechanical analysis of double pass dissimilar welds of twinning induced plasticity steel to austenitic/duplex stainless steels. Int J Press Vessels Pip. 2022;198:104665. https://www.sciencedirect.com/science/article/pii/S0308016122000564
- 52. Li H, Liu W, Chen L, et al. Investigation of sigma phase generated by simulated welding heat treatment on corrosion behavior of 2205 hydraulic control pipeline steel. Int J Press Vessels Pip. 2024;210:105240. https://doi.org/10.1016/j.ijpvp.2024.105240
- 53. Touileb K, Hedhibi AC, Djoudjou R, et al. Mechanical. microstructure, and corrosion characterization of dissimilar austenitic 316L and duplex 2205 stainless-steel ATIG welded joints. Materials. 2022;15(7):2470. https://www.mdpi.com/1996-1944/15/7/2470

How to Cite: Sharma G, Chauhan BS. Impact of High Heat Input on Micro-Structural and Mechanical Performance of SS304L/DSS2205 Steel Dissimilar GTA Weld. Int Res J Multidiscip Scope. 2025; 6(4):1157-1172. doi: 10.47857/irjms.2025.v06i04.06817